Online Data Supplement

17β-estradiol and estrogen receptor-α protect right ventricular function in pulmonary hypertension via BMPR2 and apelin

A. L. Frump, M. Albrecht, B. Yakubov, S. Breuils-Bonnet, V. Nadeau, E. Tremblay, F. Potus, J. Omura, T. Cook, A. Fisher, B. Rodriguez, R.D. Brown, K. R. Stenmark, C. D. Rubinstein, K. Krentz, D. M. Tabima, R. Li, X. Sun, N. C. Chesler, S. Provencher, S. Bonnet, T. Lahm

Supplemental Materials and Methods

All experiments were performed in accordance with recent recommendations (1-3), including randomization and blinding at the time of measurement and analysis.

Animal care

All rodents used in studies were approved by the Indiana University School of Medicine Institutional Animal Care and Use Committee (Protocol #11220) and were adherent with the National Institutes of Health guidelines for care and use of laboratory animals under the animal welfare assurance act. Rats and mice were allowed *ad libitum* access to food and water and were housed in a facility with a 12-hour light/dark cycle.

CRISPR/Cas9-mediated generation of ERα (Esr1) loss-of-function mutant rats

Two target sequences (GCCGTGTTCAACTACCCCGA**GGG** and GCTGCGCAAGTGTTACGAAG**TGG**) within the second and third exon, respectively, of the coding sequence of *Esr1* (the rat gene encoding ERα) were selected. gRNAs targeting these sequences were synthesized *via in vitro* transcription. gRNAs (25 ng/μl each) were co-microinjected with Cas9 protein (40 ng/μl) into Sprague-Dawley rat embryos, and embryos were transferred into pseudo-pregnant recipients. Weanlings from this process were sampled and *Esr1* mutations were molecularly characterized. We validated these 6 animals with loss-of-function for *Esr1* due to the introduction of non-sense mutations or chromosomal rearrangements at this locus at the transcript level in RV tissue (**Suppl. Table 1**; presumably due to disruption of the transcriptional unit and nonsense mediated decay), and characterized these animals in the HPH studies . Animals heterozygous for a 25 base pair deletion in *Esr1* exon 3 were used to establish

an ERα mutant colony, and subsequent homozygous mutant offspring were used in SuHx-PH studies.

BMPR2 Δ71 mutant rats

Rats were generated as described previously using the zinc finger nuclease method (4). WT littermates served as controls. Age-matched 6-week old male or ovariectomized female rats underwent PAB or sham surgery. A subgroup PAB rats were given E2 (75 µg/kg/day *via* subcutaneous pellets) at the time of surgery. Rats underwent closed-chest right heart catheterization with a Transonic pressure volume 1.6F catheter (Transonic, Ithaca, NY) to assess right ventricular end diastolic pressure (RVDEP), right ventricular cardiac output (CO), and echocardiography to assess pulmonary artery acceleration time (PAAT).

In vivo treatment with ML221

Male Sprague-Dawley rats (150-180g; Charles River) underwent PAB or sham surgery. A subgroup of PAB rats were given E2 (75 µg/kg/day *via* subcutaneous pellets) +/- ML221 (10 mg/kg/day *via* subcutaneous pellets; Cayman Chemical, Ann Arbor, MI; Innovative Research of America, Sarasota, FL) at the time of surgery. RV function was monitored by echocardiography.

Hemodynamic assessment and echocardiography

Hemodynamic and echocardiographic assessments were performed under isoflurane anesthesia (1-2%) as described previously (14, 68). RVSP was measured with a 2-Fr Millar catheter (Houston, TX) using LabVIEW software (National Instruments, Houston, TX). Cardiac output was derived from velocity time integral in the RV outflow tract and expressed relative to

body mass as cardiac index (CI) (15). Total pulmonary vascular resistance index (TPRI) was calculated as RVSP/CI.

RV Tissue collection

The RV free wall was cleaned in saline and weighed. The apex was fixed in 16% neutral buffered formalin for 48 hours for immunohistochemical analysis; the remainder was snap-frozen in liquid nitrogen for biochemical analysis.

Yearling steer studies

We performed studies in yearling steers since these animals provide a model of PH and RV hypertrophy that allowed us to corroborate our data obtained in rodents. Angus beef calves were born and raised at Rouse Ranch, Saratoga, WY (elevation 7120 ft/2170 m). Pulmonary artery pressures (PAP) were measured by right heart catheterization *via* the jugular vein in restrained, unsedated animals as previously described (5). At this time, two groups (n=10 each) of calves with the highest mean PAP (HPAP; 52.9 ± 5.8 mmHg, range 47-64 mmHg) and lowest mean PAP (LPAP; 35.3 ± 1.7 mmHg, range 33-38 mmHg) were selected for follow-up. Animals were maintained at the ranch under standard feed and housing conditions. PAP measurements were repeated on the study groups at twelve and thirteen months with accompanying blood collection at thirteen months. HPAP animals tended to show continuously increasing mean PAP (or progressive PH) and clinical signs of RVF; whereas LPAP animals showed constant or decreasing mean PAP (6). Five LPAP animals (physiologically adapted to altitude) and five HPAP animals (PH, maladapted to high altitude) were selected for RNA-Sequencing analysis. All experimental field procedures were performed with approval of the Colorado State University IACUC (protocol no. 09-1524A).

RNA-Seq of bovine RV

Animals were humanely euthanized at University of Wyoming Meat Science Laboratory, Laramie, WY (elevation 7165 ft/2184 m), at age 15 months in May 2013. RV tissues were collected, RNA was isolated using Trizol (Thermo Fisher) and validated for quality (RIN ≥ 7.0) using an Agilent BioAnalyzer (Santa Clara, CA). RNA libraries were constructed from total RNA using the Illumina TrueSeq (San Diego, CA), and RNA Sequencing at 100 bp single reads was performed using the Illumina HiSeq 2000. Sequencing reads, quality control, and RNASeq analysis was performed using the CLC Genomics Workbench (Qiagen Bioinformatics, Redwood City, CA) using the ENSEMBL bovine reference genome for assembly and annotation (UMD 3.1. release 77, ftp://ftp.ensembl.org/pub/release-77/genbank/bos_taurus/). Gene expression abundance, normalization, and threshold were set as Reads Per Kilobase per Million Mapped Reads (RPKM) > 0.2. Data have been deposited in the NIH GEO repository, Ascension number GSE164320.

RV endothelial cell (RVEC) isolation

RVs were dissected from male Sprague-Dawley rats, minced and digested with Collagenase II (Gibco, ThermoFisher) at 37°C for 6 hrs. Cells were then positively selected using Pan-mouse IgG Dynabeads (ThermoFisher) coated with mouse monoclonal anti-rat CD31 antibody (BD Biosciences) and then seeded on a gelatin-coated 6-well plate in EGM-2MV (Lonza) media supplemented with Normocin (Invivogen, San Diego, CA). Endothelial lineage was validated based on morphonology, von Willebrand factor stain, Matrigel tube formation, and Dio-AC-LDL uptake. Cells were utilized in experiments up to passage 7.

115 *Transwell migration and tube formation assays*

116 RVECs at 70-80% confluency were serum starved in 0.1% BSA and EBM-2 (Lonza)
117 overnight. For ML221 pretreatment, 100 nM ML221 (Cayman Chemical, Ann Arbor, Michigan) or
118 vehicle control (DMSO) was added to RVECs after serum starvation, 24 hours prior to transwell
119 migration or tube formation assay.

120 *Transwell migration assay:* $5x10^4$ RVECs were seeded onto a 24-well transwell insert
121 (Celltreat, Pepperell, MA; 8 µm pore size) containing EBM2 in the upper chamber. RVCM
122 conditioned media or EGM-2MV (as a positive control) were added to the bottom chamber of the
123 24 well plate. Each condition was performed in technical triplicate and biological quadruplicate.
124 Cells were allowed to migrate for 16 hrs, fixed with 70% EtOH and stained with Crystal violet. 15
125 fields per condition were imaged at 10x magnification using a Nikon Eclipse 80i inverted
126 microscope with camera and NIS-Elements 4.0 software (Nikon Instruments, Melville, NY) and
127 quantified using ImageJ.

128 *Tube formation assay:* $5x10^4$ RVECs were plated onto Geltrex LDEV-free phenol red-free
129 reduced growth factor basement membrane matrix (ThermoFisher) in EBM-2 basal media or
130 RVCM conditioned media for 16 hours and then 15 fields per condition were imaged at 10x
131 magnification using a Nikon Eclipse 80i inverted microscope with camera and NIS-Elements 4.0
132 software (Nikon Instruments, Melville, NY) and quantified using ImageJ. Performed in technical
133 triplicate in RVECs isolated from 4 male rats.

134

135 *Preparation of RVCM conditioned media*

136 Six hours after isolation or 24 hours post siRNA knockdown, AS serum containing media
137 (Cellutron) was replaced with AW serum-free media (Cellutron) was to RVCMs for 24 hrs. Cells
138 and conditioned media were collected, and cells were separated by centrifugation (500 x g, 2

min). Conditioned media was then strained using a 0.22 µm filter and used for RVCM conditioned media studies.

RVCM immunofluorescence

RVCMs ($5x10^3$ cells/well) were plated on BioCoat Poly-D-Lysine/Laminin coated culture slides (Corning, Bedford, MA). To verify viability, prior to plating, cells were stained with Trypan Blue solution (Corning). Cells were fixed with 4% paraformaldehyde and blocked with 3% goat serum. Primary antibodies used were rabbit polyclonal anti-ERα (1:100; Santa Cruz HC-20; Dallas, TX) and mouse monoclonal anti-α-actinin (1:800; Sigma). Secondary fluorochrome-conjugated anti-rabbit antibody (1:200; Alexa Fluor 488; Thermo Fisher), fluorochrome-conjugated anti-mouse antibody (1:200; Alexa Fluor 594; Thermo Fisher) and anti-fade DAPI (Thermo Fisher) mounting media were used. Images were taken using a Nikon Eclipse 80i microscope with camera and NIS-Elements 4.0 software (Nikon Instruments, Melville, NY) at 40x magnification.

In vitro treatment with fulvestrant (ICI 182,780)

H9c2 cells were serum starved overnight and then pretreated with the non-selective ER antagonist fulvestrant (ICI 182,780; 100 nM; Tocris, Bristol, United Kingdom) or ICI + E2 (100 nM each) for 24 hours. Cells were then treated with staurosporine (50 nM; Sigma Aldrich) for 4 hours.

siRNA experiments

RVCMs were transfected with lipofectamine RNAimax (Thermo Fisher) and Silencer Select siRNA oligos directed against apelin or scrambled control (Thermo Fisher) for 24 hours.

H9c2 were transfected at 50% confluency with lipofectamine 2000 (Thermo Fisher) and Silencer Select siRNA oligos (Thermo Fisher) directed against ERα, BMPR2, apelin or scrambled control for 24 hours as directed by the manufacturer. Knockdown of target protein was confirmed by Western blot.

In vitro E2 and ERα agonist treatment

H9c2 cells or isolated RVCMs were treated with E2 (1 nM-100 nM, Sigma), the ERα-selective agonist BTPα (7) (1-100 nM; obtained through academic collaboration with Eli Lilly; Indianapolis, IN) or ethanol vehicle control for times indicated.

Real-time RT-PCR

Total RNA was isolated from rat RVs using RNeasy Plus Fibrous Mini Kit (Qiagen; Valencia, CA). 1 µg total RNA was reverse transcribed using iScript cDNA synthesis kit (Bio-Rad, Hercules, CA). TaqMan gene expression assays for rat *Apln, Slc27a1, Acsl1, Nppa, Nppb* or *Hprt1* (assay IDs: Rn00581093_m1, Rn00585821_m1, Rn00563137_m1, Rn00664637_g1, Rn00580641_m1, and Rn01527840_m1; ThermoFisher) were used. Changes in mRNA expression were determined by the comparative CT ($2^{-\Delta\Delta C_T}$) method.

Tissue homogenization

Rat and mouse RV or LV tissue was homogenized using an Omni international tissue grinder (ThermoFisher) in ice-cold RIPA lysis buffer (Thermo Fisher) containing proteinase inhibitor cocktail (EMD-Millipore-Sigma Aldrich, St. Louis, MO) and PhosStop inhibitor cocktail

(Roche, Pleasanton, CA). After homogenization, lysate was sonicated for ten one-second pulses at 100% power and then centrifuged. The supernatant was saved and used as RV or LV lysate.

Cell lysis

RVECs and RVCMs were lysed using 10x Cell lysis buffer diluted with molecular biology grade water (ThermoFisher) and supplemented with Cell Signaling Biotechnology (Danvers, Mass) proteinase inhibitor cocktail (EMD-Millipore-Sigma Aldrich, St. Louis, MO) and PhosStop inhibitor cocktail (Roche, Pleasanton, CA). Cells were lysed using the manufacturers protocol.

Western blot analysis

Protein concentration was measured using BCA Protein Assay (Pierce-Thermo Fisher). Human RV tissue was collected and homogenized as described previously(8). For detailed antibody information see Suppl. Table 3. Rabbit polyclonal anti-ERα (1:1000; Santa Cruz HC-20; Dallas, TX), anti-ERβ (1:1000; Santa Cruz HC-150), anti-apelin (1:1000; Santa Cruz), anti-ERK1/2 (1:1000; Cell Signaling; Danvers, MA) anti-phospho-ERK1/2 (1:1000; Cell Signaling), anti-PKCε (1:1000, ThermoFisher), anti-P38 (1:1000; Cell Signaling), anti-phospho-P38 (1:1000; Cell Signaling), anti-APJ (1:1000; abcam; Cambridge, MA) and mouse monoclonal anti-BMPR2 (1:1000; BD Biosciences; Franklin Lakes, NF), and anti-Vinculin loading control (1:5000; Calbiochem; Billerica, MA) primary antibodies were used on mouse and rat RV and LV tissue homogenates. Rabbit polyclonal anti-ERα, anti-ERβ, and anti-apelin (all 1:1000, abcam) and mouse monoclonal anti-BMPR2 (1:500, BD Biosciences) were used on human RV tissue homogenates. All antibodies were diluted in Pierce Protein-Free T20 blocking buffer (ThermoFisher). Anti-Rabbit-HRP (Cell Signaling, Danvers, MA) and anti-mouse-HRP (KPL, Gaithersburg, MD) secondary antibodies were diluted 1:2000 in Pierce Protein-Free T20 Blocking

Buffer. Human RV Western blots were normalized to Amido Black stain (Sigma Aldrich). Densitometry was performed using Image J.

Assessment of hypertrophy and fibrosis in human and rat RV

Human RV sections (5 µm) were stained with hematoxylin-eosin (for RV hypertrophy) and Masson-trichrome (for fibrosis). Cardiomyocyte-cross sectional area was obtained by tracing the outlines of cardiomyocytes with a clear nucleus image in hematoxylin-eosin stained sections (5 random images and a minimum of 50 cardiomyocytes per specimen).The fibrosis area was measured on Masson-trichrome stained sections and expressed as percent of analyzed tissue sections. Analyses were performed using a Zeiss digital imaging microscopy workstation (Intelligent Imaging Innovations (3i), Denver, CO) and Image J Software (NIH, Bethesda, MD, USA).

Immunofluorescence, assessment of fluorescence intensity, and nuclear localization in human RV

Immunofluorescent labeling for ERα, apelin and apelin receptor (APLNR) was performed using formalin-fixed paraffin-embedded human RV sections 4µm thick. Antigen retrieval was performed by heating samples in 0.01 M citrate buffer (10 mM Sodium Citrate, 0.05% Tween-20, pH 6.0). ERα (1:200 dilution; rabbit polyclonal; Abcam #ab3575) or Apelin receptor (1:200 dilution; rabbit polyclonal; Lsbio LS-B14256) along with CD31 (1:50 dilution; mouse monoclonal; Dako #M0823) primary antibodies and Alexafluor 594nm (1:500 dilution; Goat anti-rabbit IgG, ThermoFisher #A11037) and Alexafluor 488 nm (1:500; Goat anti-mouse IgG, ThermoFisher #A11001) secondary antibodies were used. DAPI staining was used to visualize nuclei. Apelin primary antibody (1:1000 dilution; rabbit polyclonal; Biorbyt #orb247041), was amplified by

Tyramide signal amplification (Cy3; Perkin Elmer NEL744E001KT). Secondary biotinylated antibody was applied (1:500 dilution; Goat anti-rabbit IgG, Chemicon, #AP132B) and developed with Vectastain HRP ABC Reagent (Vector Laboratories; # PK6100). CD31 labeling was visualized in far red (CY5 (1:500 dilution; Goat anti-mouse IgG, Jackson immunoresearch #115 175 166). Negative controls were performed during each experiment by incubating secondary antibodies alone or by using rabbit IgG isotype control (1:500; SantaCruz sc-2027) and following all protocol steps including incubation with the secondary antibody. Imaging for each antibody was taken at the identical exposure time for each experimental condition/magnification. Images were acquired using a Carl Zeiss MicroImaging microscopy workstation and were quantified using Zen software.

Total fluorescence intensity was determined by measuring intensity over 20 short axis cardiomyocytes dispersed over 8 pictures per sample at 40X and divided by the area of the cardiomyocyte. For total fluorescence intensity in endothelial cells, fluorochrome intensity was measured in 8 vessels dispersed over 8 pictures per sample at 40X and divided by the area of the vessel. To quantify nuclear co-localization of ERα in cardiomyocytes, 8 pictures of transversal sections at 40X were taken and an average of 70 short axis cardiomyocytes distributed throughout the tissue were analyzed per specimen. To quantify nuclear expression in endothelial cells, 8 vessels dispersed over 8 pictures at 40X distributed throughout the tissue were analyzed by specimen by quantifying the total number of ERα positive cells and DAPI positive cells in CD31 layer. The percentage of positive labeled nuclei ((ERα +ve nuclei/ Total nuclei) * 100) was quantified. To quantify cytoplasmic-membrane expression ERα in cardiomyocytes, 20 cardiomyocytes were analyzed per specimen and nuclear expression was excluded. Total intensity (cytoplasmic and membrane) of the ERα in the cardiomyocyte was calculated and this value was divided by the area of the cardiomyocyte. For cytoplasmic-membrane expression in endothelial cells 8 vessels per sample were analyzed by manually encircle the vessel avoiding

the nuclei to obtain the intensity of the fluorochrome related to the protein of interest and the area of the vessel.

Immunohistochemistry (IHC)

Immunoperoxidase staining for apelin and apelin receptor (APLNR) in rat RV was performed using formalin-fixed, paraffin-embedded sections. Rat RV sections were heated in citrate antigen retrieval buffer (10 mM Sodium Citrate, 0.05% Tween-20, pH 6.0). Apelin or APLNR were stained (1:100, abcam; 1:500, abcam, respectively) and detected with ABC amplification using Universal Vectastain ABC kit (Vector Laboratories, Burlingame, CA).

Chromatin immunoprecipitation (ChIP) assay

Materials and protocol were provided by EMD Millipore EZ ChIP (MilliporeSigma, Burlington, MA). Cells were treated with formalin to crosslink DNA/Protein complexes. Complexes were sonicated for ten five-second pulses at 75% power and then incubated overnight with rotation at 4°C with Dynabeads (Thermo Fisher) bound with ERα (5 μg protein/ml buffer; Santa Cruz). Beads were washed four times and pulled down. Protein was digested and then DNA was PCR-amplified using primers for the estrogen response element in the *Bmpr2* promoter. RNA polymerase II binding to the *Gapdh* promoter was used as a positive control.

Immunoprecipitation (IP) assay

Cells were serum starved overnight and then treated with E2. After treatment times indicated, cells were lysed and incubated overnight with rotation in a cold room with Dynabeads (Life Technologies) bound with peroxisome proliferator-activated receptor gamma (PPAR-γ)

antibody (5 μg/ml; Santa Cruz). Beads were then washed, followed by addition of sample loading buffer directly to the beads. Samples were then boiled and run on a western blot. β-catenin antibody (1:5000, R&D Systems) was used to detect complex formation. IPs with IgG controls were used to demonstrate absence of non-specific antibody binding.

Caspase-3/7 activity assay

Caspase-3/7 activity was quantified using the CaspACE (rat tissue) or ApoTox-Glow Triplex Assay (cells; both from Promega; Madison, WI) and expressed as relative light units (RLU). Caspase-3/7 activity in RV homogenates was measured as described previously (9). H9c2 cells were pre-treated for 24 hours with E2 (1 nM - 100 nM, Sigma), the selective ERα agonist BTPα (7) (1 nM - 100 nM; obtained through academic collaboration with Eli Lilly; Indianapolis, IN), the selective ERα agonist PPT (0.1 nM - 10 nM) or ethanol or DMSO vehicle. Pro-apoptotic signaling was induced by treating cells with staurosporine (50 nM; Sigma) added to culture media for an additional 24 hours.

Statistical analysis

Results are expressed as means±SEM. Biologically-independent experiments (run in technical duplicates) were performed for all *in vitro* studies and reported as N. Statistical analyses were performed with GraphPad Prism 6 (La Jolla, CA). Sample sizes were estimated by power calculation. Student's t-test or one-way ANOVA with Tukey's or Dunnett's *post-hoc* correction was used for comparison of experimental groups. Correlations were determined using Pearson's coefficient (R). Normality testing for all data sets used in correlation analyses was performed using D'Agostini and Pearson testing as well as Shapiro-Wilk testing. Statistically significant difference was accepted at $p<0.05$.

Supplemental results

ERα activation attenuates pro-apoptotic signaling

Given our prior findings demonstrating that E2 attenuates RV pro-apoptotic signaling, we wanted to determine if ERα, in addition to regulating apelin, is also involved in mediating anti-apoptotic effects of E2. In particular, in H9c2 cells, E2 attenuated staurosporine-induced increases in activation of the stress signaling mediator P38MAPK in an ER-dependent manner (**Suppl. Fig. 9**), and two ERα agonists (BTPα or PPT) recapitulated E2's attenuating effects on pro-apoptotic signaling (caspase-3/7 activity) after staurosporine exposure (**Suppl. Fig. 10**).

Treatment with E2 upregulates BMPR2 canonical downstream signaling in RVs from PAB rats

Given our findings demonstrating that E2 increases canonical BMPR2 signaling in rat cardiomyoblasts (Suppl. Fig. 11), we set out to determine whether E2 also stimulates canonical BMPR2 signaling *in vivo*. Indeed, in male or ovariectomized (OVX) female rats undergoing PAB for 11 weeks, E2 treatment (starting at the time of PAB and continued for the entire experimental period) was associated with a significant increase in RV Id1 protein expression as well as a trend for increased Smad1/5/8 phosphorylation (**Suppl. Fig. 12**).

Supplemental Table 1

Animal number	Sex	Exon 2	Exon 3	Predicted phenotype	ERα (*Esr1*) mutation type
1081	Female	-18bp/-18bp	-10bp, -10bp	Sense, KO/ Sense, KO	Hypomorph
1082	Female	-363(TSS)/ -363	-10bp, inv	KO, KO/ KO, inv	Homozygous Null
1086	Male	-18bp/ -18bp	-10bp, -4bp	Sense, KO/ Sense, KO	Hypomorph
1087	Male	-58bp/ -58bp	Inv, inv	KO, inv/ KO, inv	Homozygous Null
1088	Male	Brkpnt/ brkpnt	Brkpnt, brkpnt	Excision/excision	Heterozygous Null
1090	Female	Inv/ inv	Inv, inv	Dupl-inv/dupl-inv	Heterozygous Null

Supplemental Table 1: CRISPR/Cas9-mediated ERα (*Esr1*) mutations in Sprague-Dawley rats. Molecular characterization results *via* PCR and sequencing, predicted allelic phenotype, and mutation type generated from targeting exon 2 and exon 3 of the *Esr1* gene (the gene encoding ERα) in male and female Sprague-Dawley rats. DNA repair events captured in our characterization assays include the introduction of indels (for which the net loss of base pairs is given), excisions between both target sites (for which the chromosomal breakpoints are listed), inversions (primers annealing the same strand anomalously generated a PCR product), and compounded duplications and inversions (inversions that gave a larger fragment than expected). Bp = base pairs; TSS = transcription start site loss; brkpnt = breakpoint; inv = inversion; sense = sense mutation; KO =non-sense mutation; dupl-inv = duplication-inversion mutation.

Supplemental Table 2: Patient Characteristics

Category	Diagnosis	Cause of death	Origin of tissue	Patient sex	Patient age (years)	Tricuspid gradient (mmHg)	RV Fibrosis (%)	RV Hypertrophy (RV myocyte cross sectional area, μm²)	mPAP (mmHg)	PAOP (mmHg)	RAP (mmHg)	PVR (WU)	CO^ (L/min)	CI^ (L/min/m²)	LVEF (%)	TAPSE (mm)	NYHA class	6MWD (m)	PAH medications
Control	Coronary artery disease	Sudden cardiac death*	Autopsy	Female	43	N/A	0.61	148.24	N/A	N/A	N/A	N/A	N/A	N/A	N/A	N/A	N/A	N/A	N/A
Control	Coronary artery disease	Sudden cardiac death*	Autopsy	Male	29	N/A	4.49	218.03	N/A	N/A	N/A	N/A	N/A	N/A	N/A	N/A	N/A	N/A	N/A
Control	Coronary artery disease	Sudden cardiac death*	Autopsy	Male	65	N/A	3.49	188.81	N/A	N/A	N/A	N/A	N/A	N/A	N/A	N/A	N/A	N/A	N/A
Control	Coronary artery disease	Sudden cardiac death*	Autopsy	Female	49	N/A	1.28	214.66	N/A	N/A	N/A	N/A	N/A	N/A	N/A	N/A	N/A	N/A	N/A
Control	Coronary artery disease	Sudden cardiac death*	Autopsy	Male	52	N/A	2.13	173.41	N/A	N/A	N/A	N/A	N/A	N/A	N/A	N/A	N/A	N/A	N/A
Control	Ross Procedure (aortic stenosis)	Not applicable (patient still alive)	Surgery	Female	42	24	N/A	N/A	N/A	N/A	N/A	N/A	N/A	N/A	63	N/A	II	N/A	N/A
Control	Coronary artery disease	Sudden cardiac death*	Autopsy	Female	48	N/A	3.01	145.61	N/A	N/A	N/A	N/A	N/A	N/A	N/A	N/A	N/A	N/A	N/A
Control	Ross Procedure (aortic stenosis)	Not applicable (patient still alive)	Surgery	Female	50	20	N/A	N/A	N/A	N/A	N/A	N/A	N/A	N/A	50	21	II-III	N/A	N/A
Control	Coronary artery disease	Sudden cardiac death*	Autopsy	Male	28	N/A	N/A	N/A	N/A	N/A	N/A	N/A	N/A	N/A	N/A	N/A	N/A	N/A	N/A
RVF	Pulmonary valve regurgitation#	Not applicable (patient still alive)	Surgery	Female	46	14	N/A	N/A	N/A	N/A	0-5	N/A	3.29	1.73	60	22	II	N/A	N/A
RVF	Ventricular septal defect	Cerebro-vascular accident	Autopsy	Female	57	125	18.68	390.40	N/A	N/A	5-10	N/A	2.79	1.74	60	17	N/A	419	N/A
RVF	Ventricular septal defect	N/A	Surgery	Male	61	N/A	N/A	N/A	N/A	N/A	10-15	N/A	N/A	N/A	55	N/A	II	N/A	N/A
RVF	iPAH	RVF**	Autopsy	Female	40	N/A	N/A	N/A	N/A	N/A	N/A	N/A	N/A	N/A	N/A	N/A	N/A	N/A	N/A
RVF	iPAH	RVF**	Autopsy	Female	43	N/A	N/A	N/A	N/A	N/A	N/A	N/A	N/A	N/A	N/A	N/A	N/A	N/A	Sildenafil, epoprostenol
RVF	iPAH	RVF**	Autopsy	Male	45	N/A	N/A	N/A	N/A	N/A	N/A	N/A	N/A	N/A	N/A	N/A	N/A	N/A	Bosentan, sildenafil
RVF	iPAH	RVF**	Autopsy	Female	74	94	N/A	N/A	35	10	4	6.8	4.1	2.5	55	N/A	IV	186	Bosentan
RVF	SSc-PAH	RVF**	Autopsy	Female	54	N/A	34.63	728.84	48	15	22	4.93	3.7	1.9	60	17	IV	180	Bosentan, sildenafil
RVF	SSc-PAH	RVF**	Autopsy	Male	77	N/A	13.08	291.76	47	9	7	7.86	5.4	3.2	50	13	III	230	Bosentan, sildenafil
RVF	SSc-PAH	RVF**	Autopsy	Female	47	N/A	20.29	457.18	46	7	10	6.93	3.9	2.1	60	12	III	276	Ambrisentan, tadalafil, epoprostenol

Abbreviations: CO = cardiac output; CI = cardiac index; iPAH = idiopathic pulmonary arterial hypertension; LVEF = left ventricular ejection fraction; mPAP = mean arterial pressure; N/A = not available; NYHA = New York Heart Association; PAOP = pulmonary artery occlusion pressure; RAP = right atrial pressure; PVR = pulmonary vascular resistance; RVF = RV failure; SSc-PAH = scleroderma-associated pulmonary arterial hypertension; TAPSE = tricuspid annular plane systolic excursion; WU = Wood units; 6MWD = six minute walk distance.

Echocardiography, NYHA and 6MWD data in control patients were determined at the time of surgery. For RVF patients, most recent echocardiography, right heart catheterization, NYHA and 6MWD data were used. RV fibrosis and RV myocyte cross sectional area were determined *post mortem*.

^ Hemodynamic measures may have been obtained several months prior to the patient's death and thus may not demonstrate CO/CI consistent with RVF. RVF at the time of death was determined by decreased TAPSE and/or a clinical course consistent with development of RVF.

Pulmonary valve regurgitation following previous surgical correction of Fallot Tetralogy.

* Early autopsies performed following sudden deaths. None of those subjects had any past medical history. Autopsy revealed severe left main coronary artery and/or left anterior descending artery atherosclerosis with no other cause of death. Moreover, there were no macroscopic signs of chronic right or left heart dysfunction. All subjects exhibited normal heart size, no heart hypertrophy (left and right ventricle wall diameter of 1.3-1.5 cm and 0.2-0.5 cm, respectively) and normal pulmonary arteries. In the absence of other causes, deaths were assumed related to the severe coronary artery disease observed in those patients.

** Early autopsies performed following deaths. RVF at the time of death was confirmed by decreased TAPSE and/or a clinical course consistent with development of RVF.. Presence of RV failure and RV hypertrophy confirmed during autopsy. Evidence of left heart pathology was excluded during autopsy.

343 **Supplemental Table 3. Detailed Antibody Information**

Antibody	Vendor	Catalog	Clone	Source
ERalpha	Abcam	Ab3575		Rabbit
Apelin	Abcam	Ab181786		Rabbit
Apelin	Santa Cruz	sc33804	FL-77	Rabbit
Vinculin	Calbiochem/Millipore/Sigma	Cp74	V284 or VLN01	Mouse
Phospho-ERK1/2	Cell Signaling	4376s	20g11	Rabbit
ERK1/2	Cell Signaling	4695s	137f5	Rabbit
PKC epsilon	ThermoFisher	Ma5-32715	JA38-21	Rabbit
ER alpha	Santa Cruz	Sc-543	Hc-20	Rabbit
Beta actin	Sigma	A5316		Mouse
BMPR2	BD Biosciences	612262		Mouse
Beta catenin	Millipore/Sigma	06-734		Rabbit
PPAR gamma	Santa Cruz	Sc7273x	E-8	Mouse
ER beta	Abcam	Ab3576		Rabbit
Apelin receptor	Abcam	Ab84296		Rabbit
Phospho-P38	Cell Signaling	4511s	D3f9	Rabbit
P38	Cell Signaling	9212s		Rabbit
Phospho-Smad 1/5/9	Cell Signaling	13820s	D5b10	Rabbit
Smad1	Cell Signaling	9743S		Rabbit
Id1	Santa Cruz	Sc-488	c-20	Rabbit
Apelin	Biorbyt	Orb247041		Rabbit
Apelin receptor	Ls-bio	Ls-b14256		Rabbit
CD31	Dako	M0823		Mouse
Alexafluor 488	ThermoFisher	A11001		Mouse
Alexafluor 594	ThermoFisher	A11037		Rabbit
Goat antimouse igg	Chemicon	Ap132b		Rabbit
Goat antimouse igg cy5	Jackson immunoresearch	115 175 166		Mouse
Rabbit igg isotype control	Santa cruz	Sc-2027		Rabbit
Anti-rabbit-hrp	Cell signaling	7074		Goat
Anti-mouse-hrp	KPL	5220-0288 (04-18-18)		Goat
Alpha actinin	Sigma	A7811	EA-53	Mouse

344

345

346

References

1. Provencher S, Archer SL, Ramirez FD, Hibbert B, Paulin R, Boucherat O, et al. Standards and Methodological Rigor in Pulmonary Arterial Hypertension Preclinical and Translational Research. *Circ Res.* 2018;122(7):1021-32.
2. Lahm T, Douglas IS, Archer SL, Bogaard HJ, Chesler NC, Haddad F, et al. Assessment of Right Ventricular Function in the Research Setting: Knowledge Gaps and Pathways Forward. An Official American Thoracic Society Research Statement. *Am J Respir Crit Care Med.* 2018;198(4):e15-e43.
3. Bonnet S, Provencher S, Guignabert C, Perros F, Boucherat O, Schermuly RT, et al. Translating Research into Improved Patient Care in Pulmonary Arterial Hypertension. *Am J Respir Crit Care Med.* 2017;195(5):583-95.
4. Hautefort A, Mendes-Ferreira P, Sabourin J, Manaud G, Bertero T, Rucker-Martin C, et al. Bmpr2 Mutant Rats Develop Pulmonary and Cardiac Characteristics of Pulmonary Arterial Hypertension. *Circulation.* 2019;139(7):932-48.
5. Holt TN, and Callan RJ. Pulmonary arterial pressure testing for high mountain disease in cattle. *Vet Clin North Am Food Anim Pract.* 2007;23(3):575-96, vii.
6. Neary JM, Garry FB, Holt TN, Brown RD, Stenmark KR, Enns RM, et al. The altitude at which a calf is born and raised influences the rate at which mean pulmonary arterial pressure increases with age. *J Anim Sci.* 2015;93(10):4714-20.
7. Chalmers MJ, Wang Y, Novick S, Sato M, Bryant HU, Montrose-Rafizdeh C, et al. Hydrophobic Interactions Improve Selectivity to ERalpha for Ben-zothiophene SERMs. *ACS Med Chem Lett.* 2012;3(3):207-10.
8. Potus F, Ruffenach G, Dahou A, Thebault C, Breuils-Bonnet S, Tremblay E, et al. Downregulation of MicroRNA-126 Contributes to the Failing Right Ventricle in Pulmonary Arterial Hypertension. *Circulation.* 2015;132(10):932-43.

9. Petrache I, Fijalkowska I, Medler TR, Skirball J, Cruz P, Zhen L, et al. alpha-1 antitrypsin inhibits caspase-3 activity, preventing lung endothelial cell apoptosis. *Am J Pathol.* 2006;169(4):1155-66.

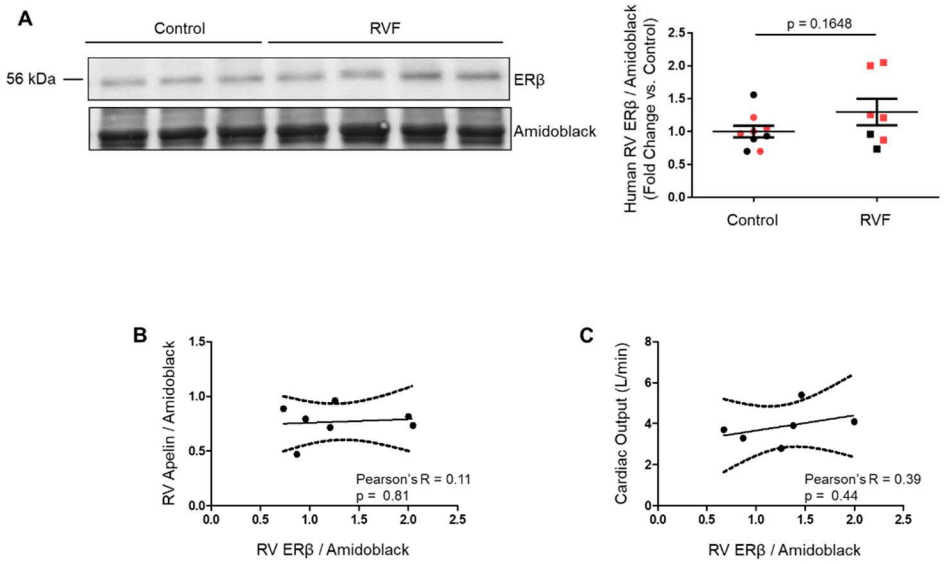

390

391 **Supplemental Figure 1: ERβ expression is not altered in RVs from patients with RV failure**
392 **(RVF) and does not correlate with apelin or RV function**. (**A**) Western blot analysis of ERβ
393 expression in human control and failing RVs. A representative Western blot is shown.
394 Densitometry includes data from all subjects. Red and black symbols in graphs represent samples
395 from female and male patients, respectively. Error bars represent means ± SEM. Blot is from the
396 same gel as Fig. 2A of the main manuscript. (**B**) ERβ does not correlate with apelin expression
397 or (**C**) cardiac output in RVF patients. Correlation analyses were performed by determining
398 Pearson's correlation coefficient (R) and two-tailed p-value. Dashed lines represent 95%
399 confidence intervals.

400

401

402

403

404

A

PH model	CO (ml/min)	Percent change from control	RV/(LV+S)	Percent change from control	RVSP (mmHg)	Percent change from control	RV end-diastolic diameter (mm)	Percent change from control
Normoxia (control)	222.2 ± 46.41	-	0.26 ± 0.01	-	25 ± 2	-	n/a	n/a
SuHx (adaptive)	186.3 ± 7.387	-16.1%	0.40 ± 0.07*	+36.5%	46.67 ± 10.26	+46.4%	n/a	n/a
SuHx (maladaptive)	87.45 ± 8.327*^	-60.6%	0.66 ± 0.08*^	+61.4%	64.33 ± 13.58*	+61.1%	n/a	n/a
Control	217.9 ± 26.93	-	0.23 ± 0.02	-	20.25 ± 2.63	-	n/a	n/a
MCT (adaptive)	143.3 ± 7.86	-34.2%	0.31 ± 0.12	+27.7%	36.5 ± 15.89	+44.5%	n/a	n/a
MCT (maladaptive)	90.06 ± 12.17*	-58.7%	0.65 ± 0.10*^	+65.2%	63.25 ± 14.57*	68%	n/a	n/a
Sham (control)	308.5 ± 58.95	-	0.23 ± 0.02	-	22 ± 1.414	-	2.715 ± 0.3416	-
PAB (adaptive)	138.1 ± 54.85*	-55.2%	0.32 ± 0.16	+29%	23 ± 4.163	+4.3%	3.179 ± 0.111	+14.6%
PAB (maladaptive)	99.67 ± 23.13*	-67.7%	0.59 ± 0.10*^	+61.3%	47.25 ± 9.069*^	+53.4%	4.673 ± 0.741*^	+41.9%

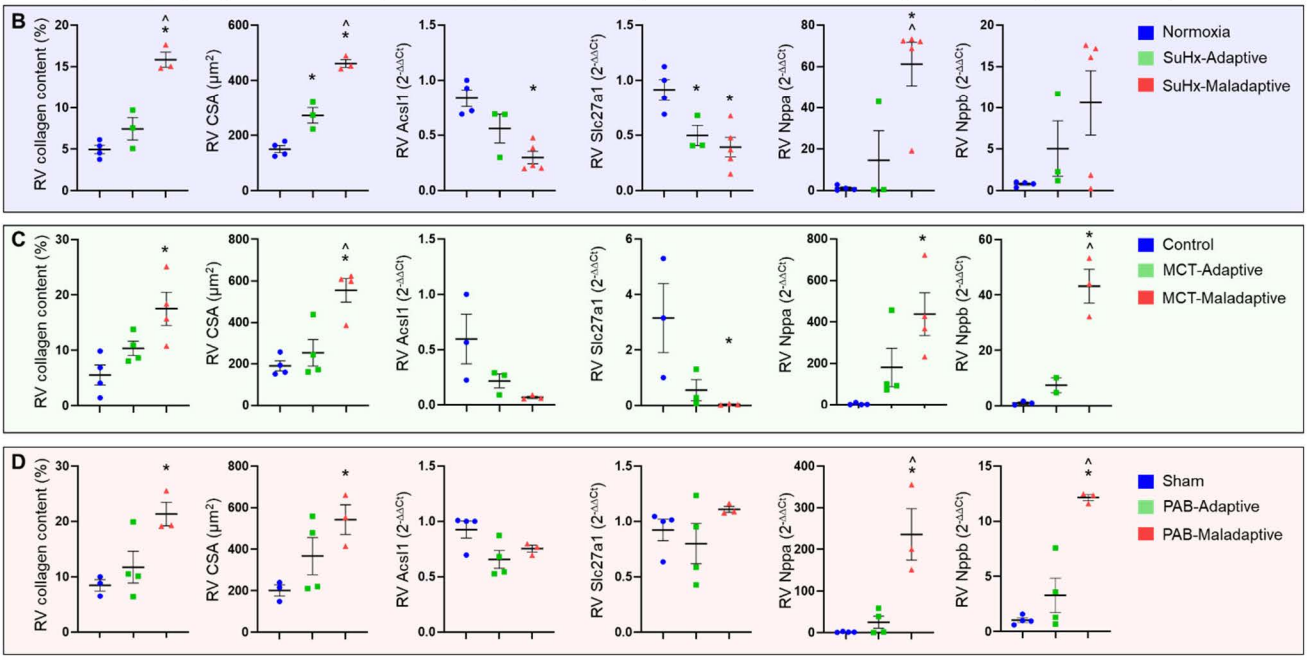

Supplemental Figure 2: Hemodynamic, structural and molecular characterization of adaptive and maladaptive RV remodeling in various models of RV pressure overload. (**A**) Identification of changes in cardiac output (CO), RV hypertrophy (RV/LV+S; right ventricle weight / left ventricle weight + septum weight), RV systolic pressure (RVSP) and RV dilation (RV end-diastolic diameter) in male rats with SuHx-PH, MCT-PH or PAB (N=3 per group). (**B-D**) Quantification of RV collagen content (via Trichrome stain), RV cardiomyocyte hypertrophy (via assessment of cell surface area [CSA]) and mRNA expression of genes involved in fatty acid synthesis (*Acsl1, Slc27a1*) or neurohormonal activation (*Nppa, Nppb*; all via real-time RT-PCR) in (**B**) SuHx-PH, (**C**) MCT-PH and (**D**) PAB rats with adaptive or maladaptive RV remodeling as well as control rats. *p<0.05 vs control, ^p<0.05 vs adaptive by one-way ANOVA with Tukey post-hoc correction. Each data point represents one animal. Error bars represent means ± SEM. n/a = not available, Acsl1 = Acyl-CoA synthetase long chain family member 1), Slc27A1 = Solute carrier family 27 member 1/ Long-chain fatty acid transport protein 1), Nppa = atrial natriuretic peptide, Nppb = B-type natriuretic peptide.

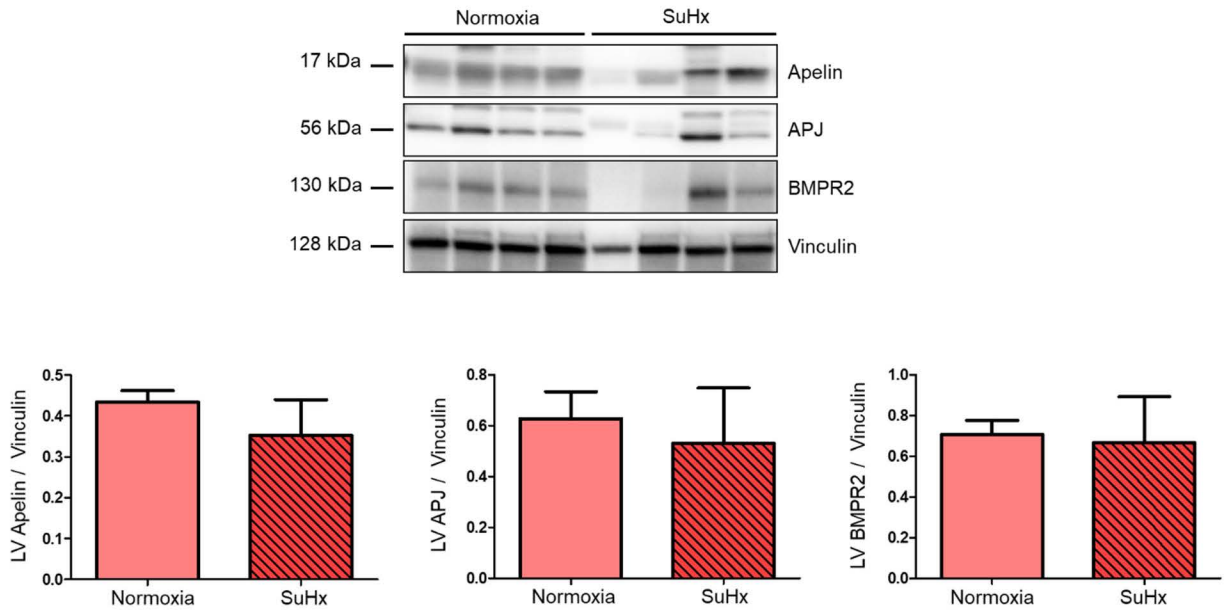

436

437

438

439 **Supplemental Figure 3: Lack of PH-induced changes in apelin and BMPR2 in the left**
440 **ventricle (LV).** Western blot analyses of apelin, apelin receptor APJ and BMPR2 in LV
441 homogenates from normoxia control or SuHx-PH female rats. N= 4 per group. Values expressed
442 as means ± SEM.

443

444

445

446

447

448

449

450

451

452

453

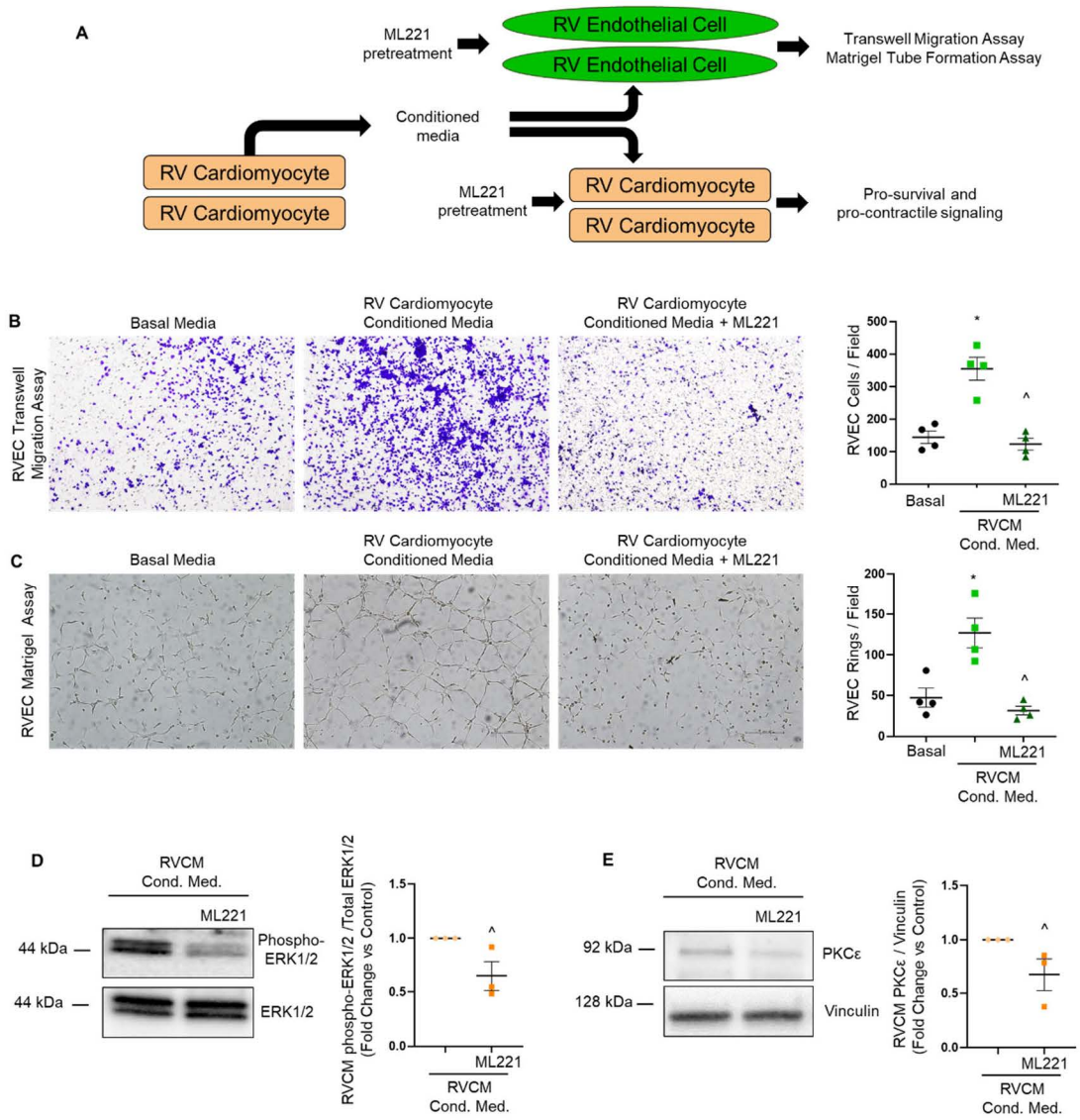

Supplemental Figure 4: Inhibition of apelin receptor (APLNR) signaling abrogates RV cardiomyocyte (RVCM) paracrine effects on RV endothelial cell (RVEC) and RVCM function. (**A**) RVCM conditioned media experimental design. Conditioned media was collected from RVCMs 24 hours after isolation and added to RVECs or RVCMs in absence or presence of pretreatment with APLNR antagonist ML221 (100 nM, 4hrs). (**B, C**) Effects of intact apelin signaling on RVEC function were evaluated by transwell migration assay and matrigel ring formation assay. (**B**) demonstrates representative transwell migration assay images of RVECs treated with basal media or RVCM conditioned media in absence or presence of ML221.

Quantification of transwell migration is shown on the right. EBM2 media served as baseline control. Images are at 4x magnification. 15 fields per condition were quantified. N = RVECs from 4 male rats, performed in technical triplicate. (**C**) depicts representative images of matrigel ring formation assay in RVECs treated with basal media or RVCM conditioned media in absence or presence of ML221. Quantification of ring formation is shown on the right. Cells were plated at a density of 5x104 in technical triplicate. 16 hours later, representative images were taken at 4x magnification and rings were quantified in 15 fields per condition. N = RVECs from 4 male rats, performed in technical triplicate. (**D-E**) Effects of APLNR blockade on RVCM pro-survival and pro-contractile signaling were evaluated using conditioned media on RVCM in absence or presence of ML221 pretreatment. Apelin downstream targets ERK1/2 (**D**) and PKCε (**E**) were evaluated by Western blot and densitometric quantification. N = RVCMs from 3 male rats, performed in technical triplicate. *p<0.05 vs basal control, ^p<0.05 vs RVCM conditioned media alone by one-way ANOVA with post-hoc Tukey's correction. Each data point represents cells from one animal. Error bars represent means ± SEM.

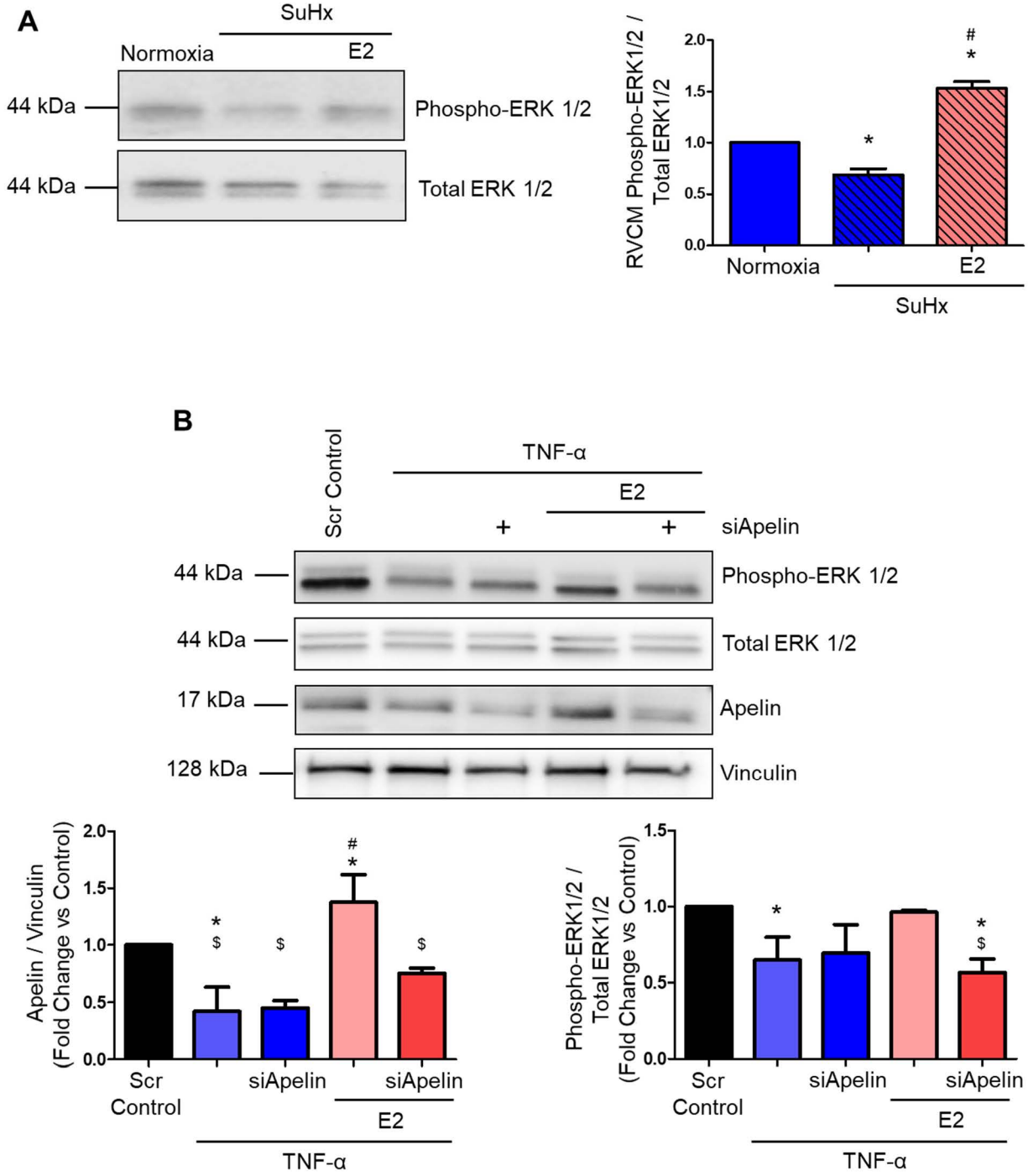

481

482

483

484

Supplemental Figure 5: Apelin is necessary for E2-mediated stimulation of pro-survival effector ERK1/2. (**A**) RV cardiomyocytes (RV CM) isolated from male SuHx-PH rats treated with E2 (75 µg/kg/day) exhibit increased phospho-ERK1/2 vs. RV cardiomyocytes from untreated SuHx-PH rats. N=4/group. (**B**) Effects of siRNA directed against apelin (5 nM) in H9c2 cardiomyoblasts pre-treated with E2 (100 nM) for 24 hrs and then stressed with TNF-α (10 ng/ml; 8 hrs). siRNA knockdown of apelin was performed 24 hrs prior to E2 treatment. N=3 independent experiments. All panels demonstrate representative Western blots with densitometric analyses for all animals or experiments. Scr = scramble siRNA control. *p<0.05 vs. Normoxia control (A) or vs. Scr control (B), #p<0.05 vs. untreated SuHx-PH (A) and vs. TNF-treated (B), $p<0.05 vs. TNF+E2 (B) by one-way ANOVA with post-hoc Tukey's correction. Values expressed as means ± SEM.

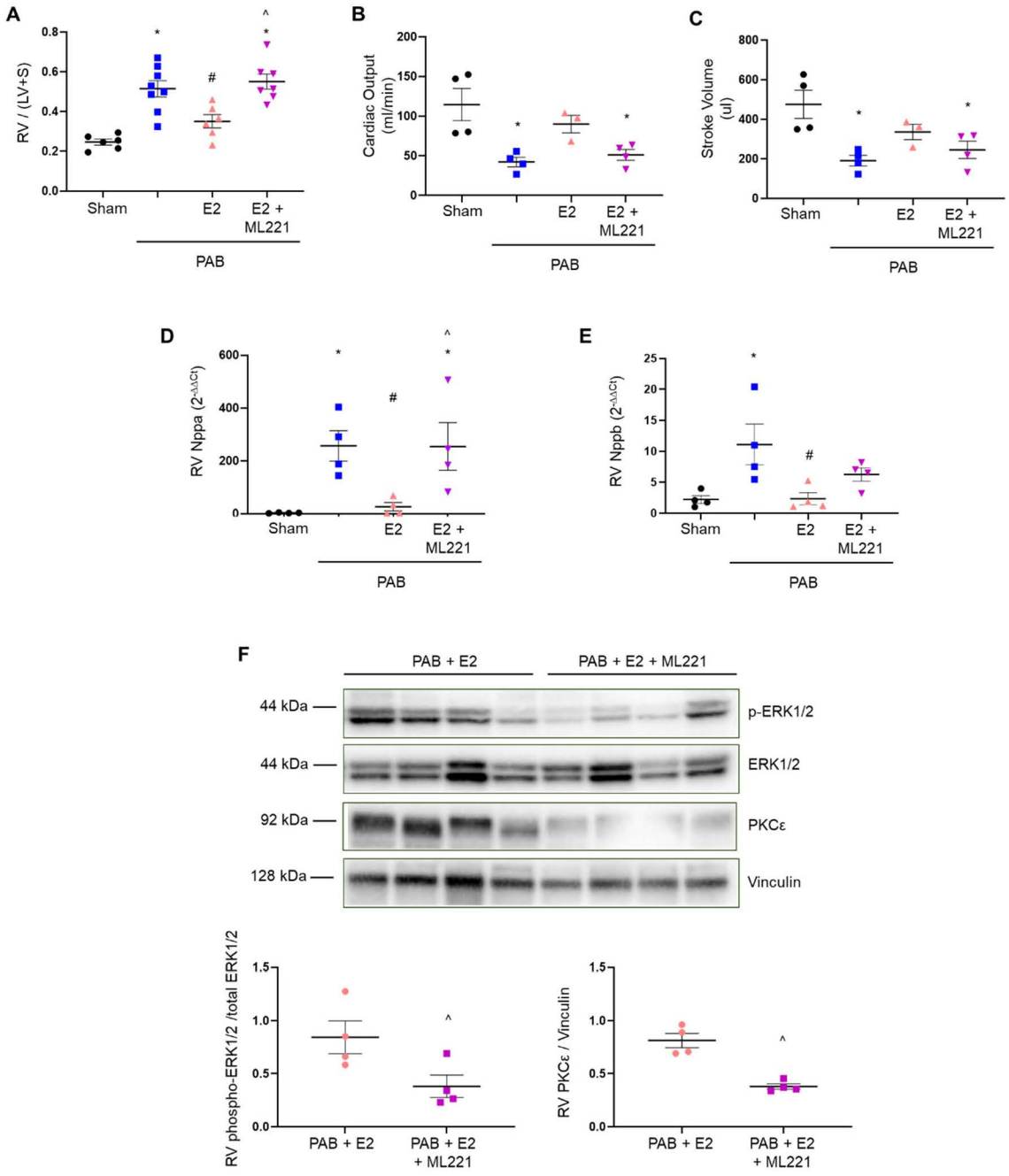
A
RV / (LV+S)
Sham
E2
E2 + ML221
PAB
B
Cardiac Output (ml/min)
C
Stroke Volume (ul)
D
RV Nppa (2^-ΔΔCt)
E
RV Nppb (2^-ΔΔCt)
F
PAB + E2
PAB + E2 + ML221
44 kDa
p-ERK1/2
ERK1/2
92 kDa
PKCε
128 kDa
Vinculin
RV phospho-ERK1/2 /total ERK1/2
RV PKCε / Vinculin
PAB + E2 + ML221

Supplemental Figure 6: Apelin signaling is necessary for E2 to exert RV-protective effects *in vivo*. Male Sprague-Dawley rats underwent pulmonary artery banding (PAB) or sham procedure. Subgroups of PAB animals received E2 (75 ug/kg/d via subcutaneous [sq] pellets) in absence or presence of APLNR antagonist ML221 (10 ug/kg/d via sq pellets) starting at the time of PAB. Animals were sacrificed after 13 weeks. E2 and ML221 were given throughout the entire duration of the experiment. (**A-C**) Effects of E2 ± ML221 treatment on RV hypertrophy (measured as weight of RV divided by weight of left ventricle plus septum; RV / [LV+S]), cardiac output, and stroke volume. Cardiac output and stroke volume were determined by pressure-volume loop assessment. (**D-E**) Assessment of RV neurohormonal activation by real-time RT-PCR. *Nppa* = atrial natriuretic peptide, *Nppb* = B-type natriuretic peptide. (**F**) Western blot analysis and densitometric quantification of apelin downstream inotropic and pro-survival mediators p-ERK and PKCε in RV homogenates of rats treated with E2 ± ML221. *p<0.05 vs sham, #p<0.05 vs. untreated PAB, ^p<0.05 vs PAB+E2 by one-way ANOVA with Tukey or Dunnett's post-hoc correction. Each data point represents one animal. Error bars represent means ± SEM.

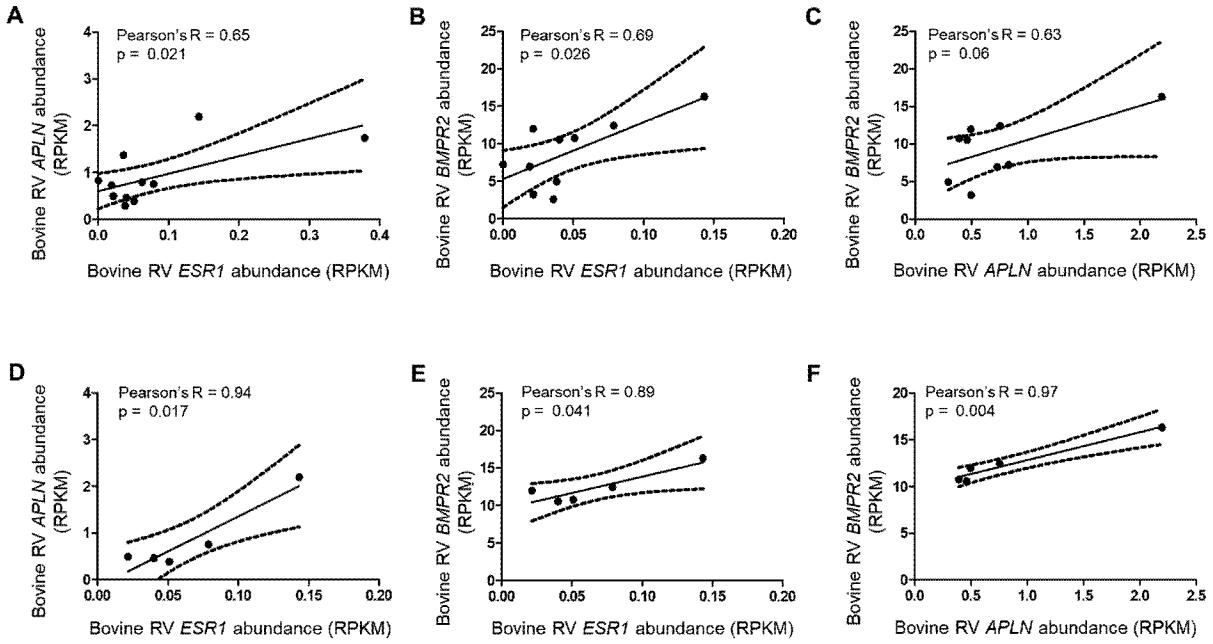

Supplemental Figure 7: Correlations between ERα, apelin and BMPR2 expression (by RNA-Seq) in RVs from yearling steers raised at high elevation. Studies were performed in the entire group of animals (steers with and without PH) as well as in the subset of steers with PH and RV failure. (**A-C**) Correlations between ESR1 (ERα), APLN (Apelin) and BMPR2 mRNA in RVs from steers with or without high-altitude induced PH. (**D-E**) Correlations between ESR1, APLN and BMPR2 mRNA in RVs from steers with PH only. Note more robust correlations in the PH group. RPKM = reads per kilobase per million mapped reads. Analyses were performed by determining Pearson's correlation coefficient (R) and two-tailed p-value. Dashed lines represent 95% confidence intervals.

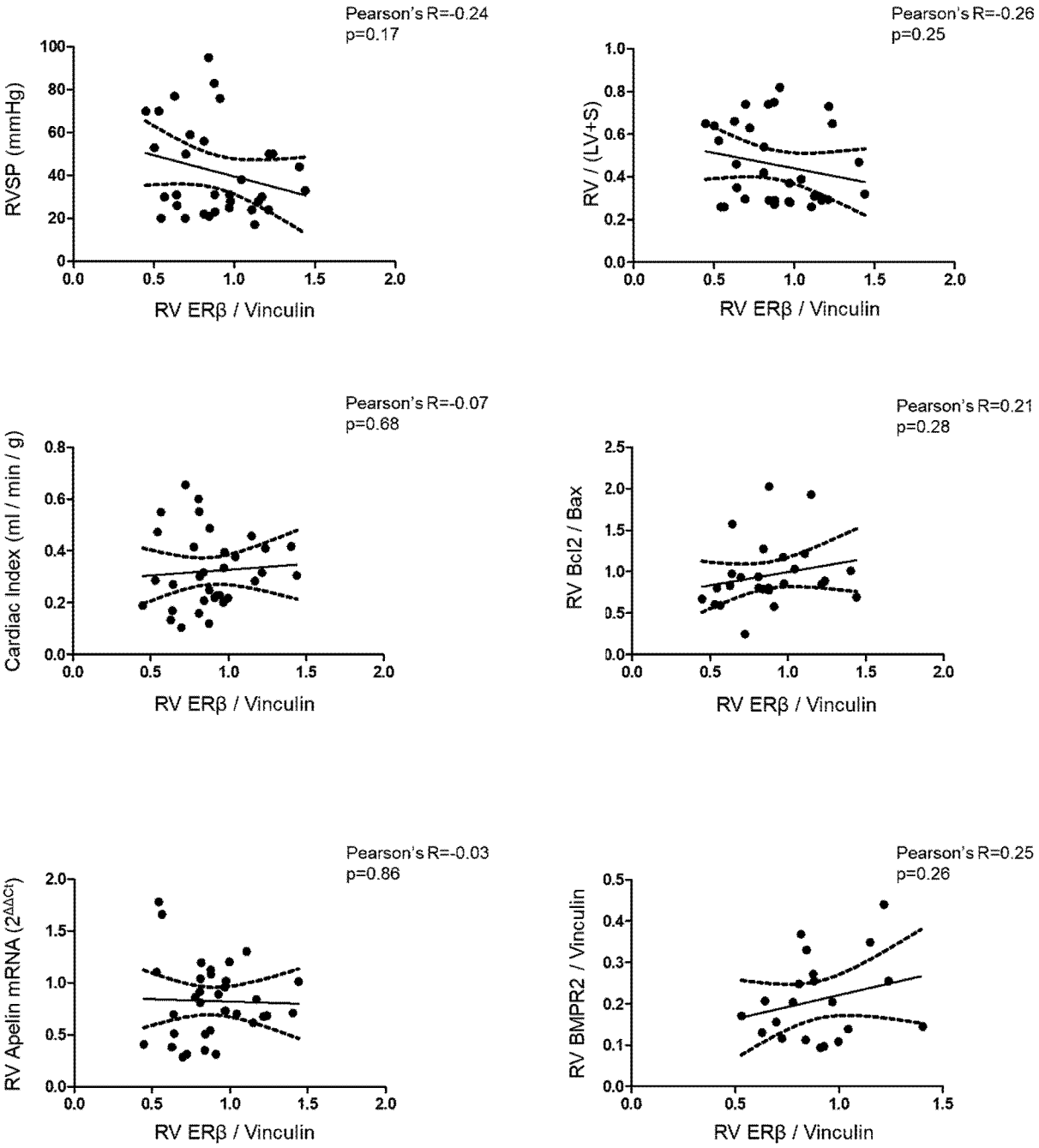

548

549

550

551

552

Supplemental Figure 8. ERβ does not correlate with parameters of RV function. RV ERβ protein expression (determined by Western blot) in male and female normoxic control or SuHx-PH rats does not correlate with RV systolic pressure (RVSP), RV hypertrophy (Fulton index; RV/(LV + S)), cardiac index or pro-survival signaling (Bcl2/Bax ratio by Western blot), or with RV apelin or BMPR2 expression. SuHx-PH animals include intact male and female SuHx-PH rats, ovariectomized SuHx-PH females, and ovariectomized SuHx-PH females replete with E2 (75 μg/kg/day). Analyses were performed by determining Pearson's correlation coefficient (R) and two-tailed p-value. Dashed lines represent 95% confidence intervals.

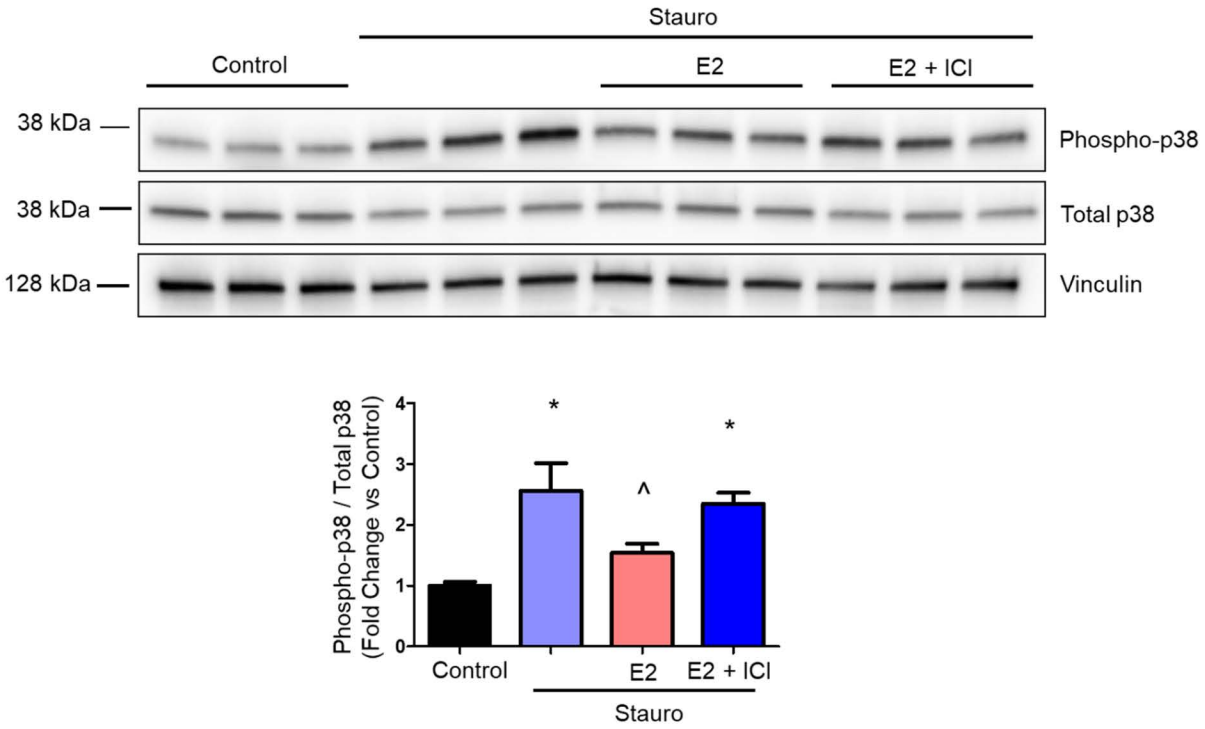

574

575 **Supplemental Figure 9: E2 attenuates staurosporine-induced stress signaling in H9c2 cells**
576 **in an ER-dependent manner.** Western blot analysis and densitometry of stress response
577 mediator phospho-p38MAPK in H9c2 cells treated with staurosporine, E2 or ER-antagonist
578 fulvestrant (ICI 182,780). Staurosporine (50 nM, 4 hrs) induces phoshpo-p38MAPK, whereas E2
579 pretreatment (100 nM, 24 hrs) reduces phospho-P38MAPK expression; these changes are
580 attenuated after ER antagonism with fulvestrant (labelled as "ICI"; 100 nM, 24 hrs.) *p<0.05 vs.
581 control; ^p<0.05 vs. stauro and E2 + ICI (one-way ANOVA with post-hoc Dunnett's correction).
582 N=3 independent experiments. Values expressed as means ± SEM.

583

584

585

586

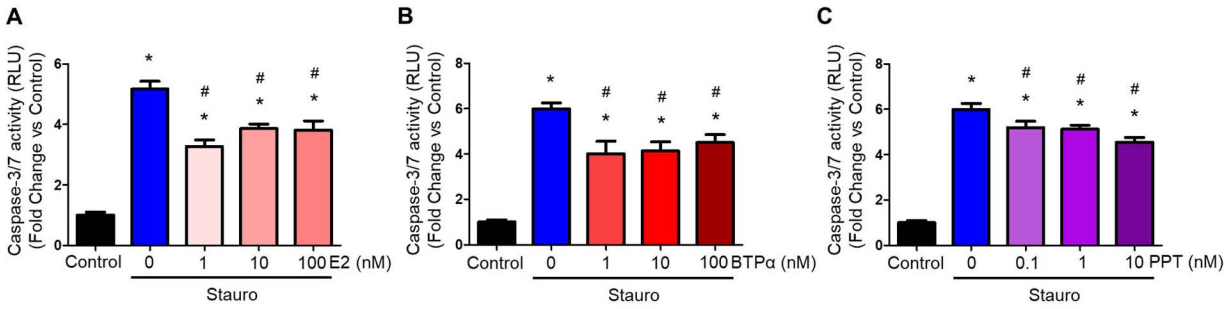

587

588 **Supplemental Figure 10: E2 or ERα agonists BTPα and PPT attenuate staurosporine-**
589 **induced pro-apoptotic signaling in H9c2 cells.** Cells were treated with (**A**) E2 (1-100 nM; 24
590 hrs), (**B**) BTPα (1-100 nM; 24 hrs) or (**C**) PPT (0.1-10 nM; 24 hrs) followed by staurosporine (50
591 nM, 24 hrs), and caspase-3/7 activity was measured (expressed in relative light units [RLU]).
592 EtOH (E2) or DMSO (BTPα, PPT) were used as vehicle controls (labelled as "0"). *p<0.05 vs.
593 control (no staurosporine), #p<0.05 vs. vehicle-treated staurosporine group by one-way ANOVA
594 with post-hoc Dunnett's test. N=3 independent experiments. Values expressed as means ± SEM.

595

596

597

598

599

600

601

602

603

604

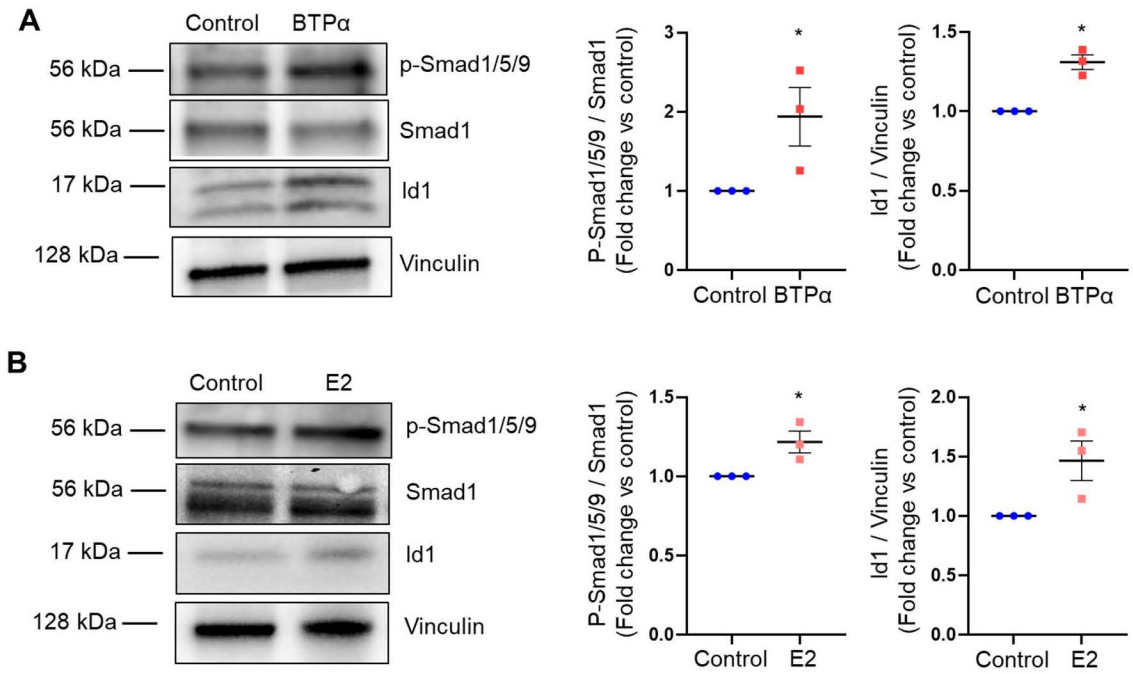

Supplemental Figure 11: Treatment with E2 or ERα agonist upregulates BMPR2 downstream signaling in rat cardiomyoblasts. (**A**) Effects of treatment with ERα agonist BTPα (100 nM, 24 hrs) on phospho-Smad1/5/9 and Id1 expression in H9c2 rat cardiomyoblasts analyzed by Western blot. (**B**) Phospho-Smad1/5/9 and Id1 protein expression in H9c2 cells treated with E2 (10 nM, 24 hrs) analyzed by Western blot. Figures depict representative Western blots with densitometric analyses for all experiments. *p<0.05 vs. untreated control by Student's t-test. N = 3 independent experiments. Error bars represent means ± SEM.

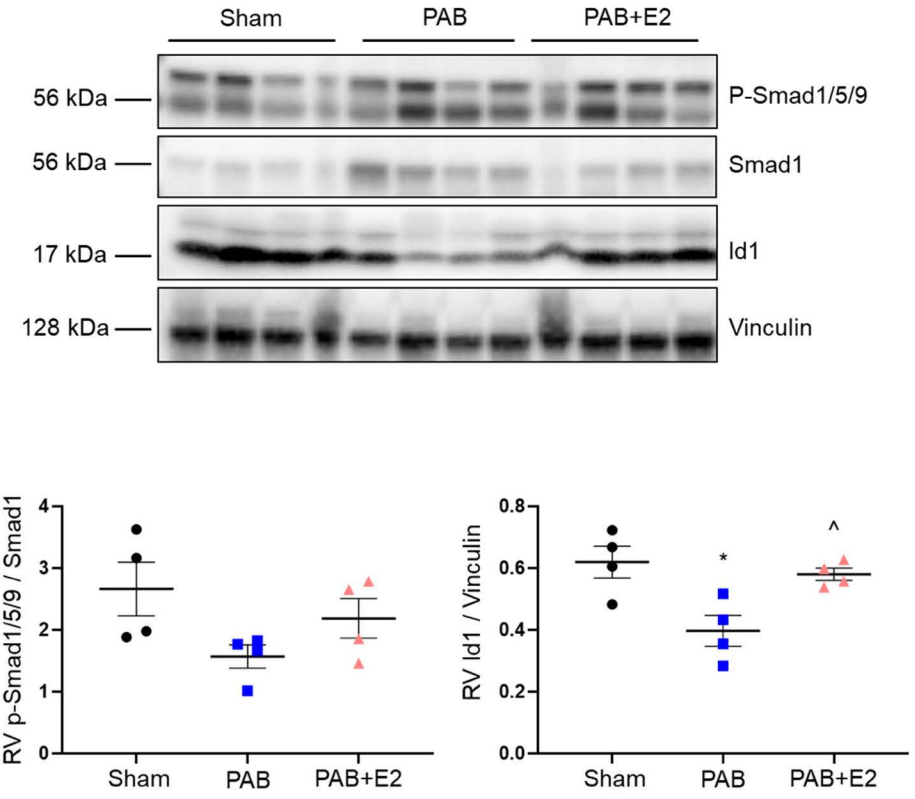

Supplemental Figure 12: Treatment with E2 upregulates BMPR2 downstream signaling in RVs from male or ovariectomized (OVX) female rats undergoing pulmonary artery banding (PAB). Animals were treated with E2 (75 µg/kg/day via subcutaneous pellets) starting at the time of PAB. Treatment was continued for a total of 11 weeks. Note increased RV Id1 protein expression and trend for increased Smad1/5/9 phosphorylation with E2 treatment. *p<0.05 vs sham, ^p<0.05 vs untreated PAB by ANOVA with post-hoc Tukey correction. Each data point represents one animal. Error bars represent means ± SEM.

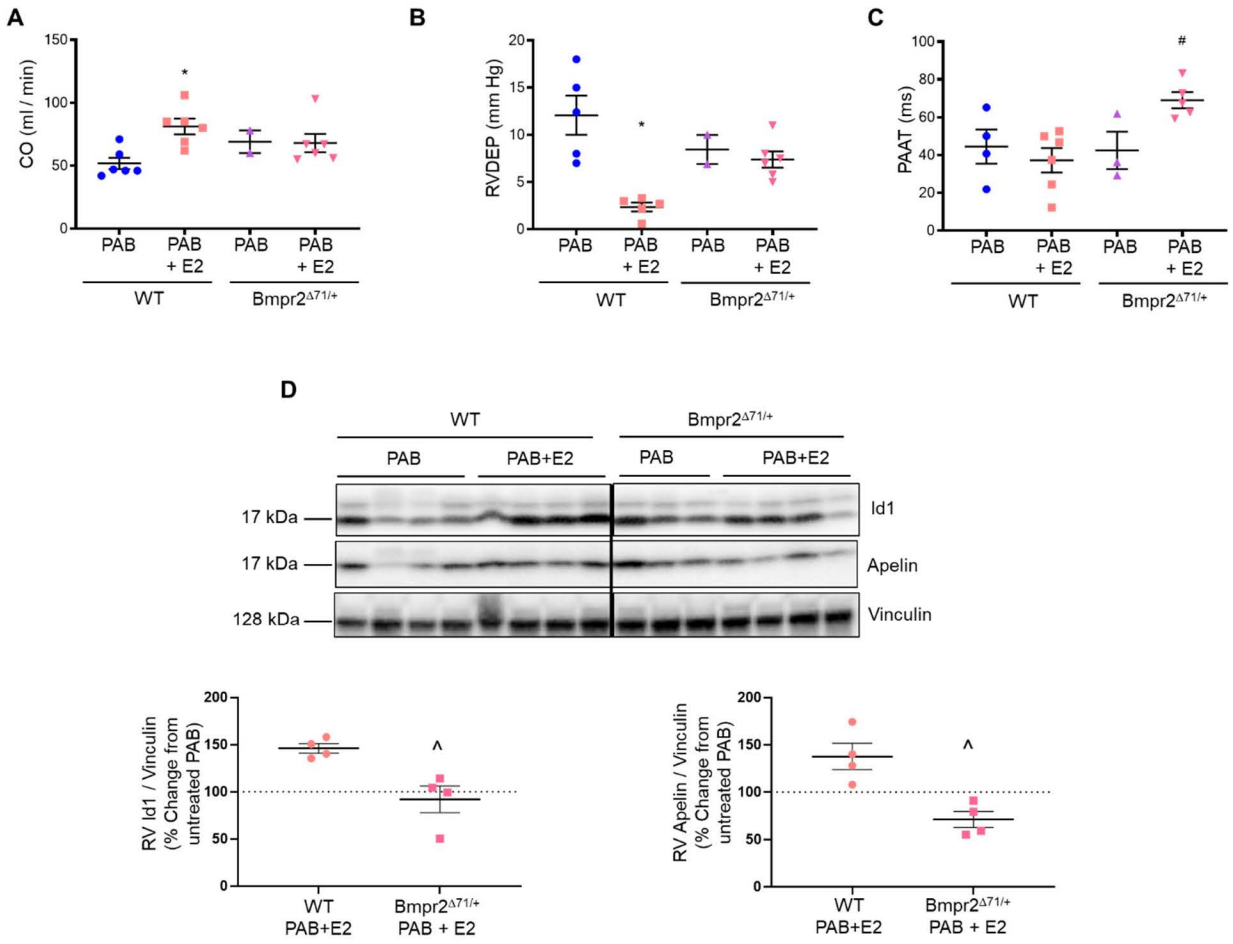

Supplemental Figure 13: BMPR2 is necessary for E2-mediated protection against RV failure induced by pulmonary artery banding (PAB). Male or ovariectomized female wild-type (WT) or Bmpr2Δ71/+ mutant rats underwent PAB with or without E2 (75 ug/kg/day via subcutaneous pellets for a total of 10 weeks). (**A-C**) Effects of Bmpr2Δ71/+ mutation on E2-mediated changes in RV cardiac output (CO; **A**), RV end-diastolic pressure (RVEDP; **B**) and pulmonary artery acceleration time (PAAT; **C**). Note lack of E2-mediated increase in CO and lack of E2-mediated decrease in RVEDP in Bmpr2Δ71/+ mutant rats as well as E2-mediated increase in PAAT in mutant rats. *p<0.05 vs PAB WT, #p<0.05 vs WT PAB+E2 by one-way ANOVA with Tukey post-hoc correction. Each data point represents one animal. (**D**) Western blot and

densitometric analysis demonstrate decreased ability of E2 to mediate increases in RV Id1 and apelin in Bmpr2Δ71/+ mutant rats (data expressed as fold-change increase in RV Id1 or apelin with E2 vs untreated). Representative images were run on the same gel but were noncontiguous, indicated by the black line. ^p<0.05 vs. WT by Student's t-test. Error bars represent means ± SEM.

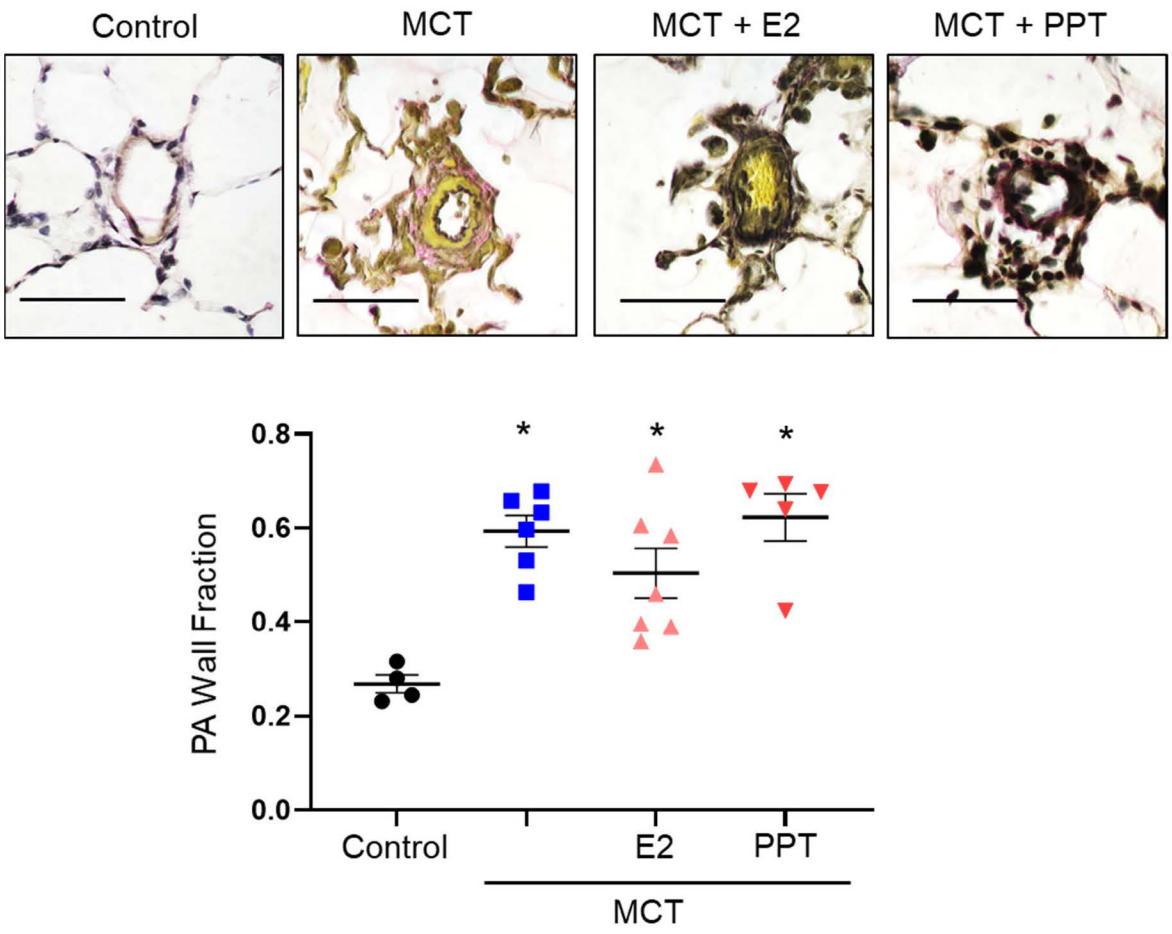

Supplemental Figure 14: Rescue treatment with E2 or ERα agonist PPT in male MCT rats does not affect pulmonary artery (PA) remodeling. E2 or PPT were given for 2 weeks (starting 2 weeks after MCT administration) as outlined in Fig. 11. PA remodeling was assessed by Verhoeff-Van Giesson staining and subsequent determination of PA wall fraction ([vessel diameter – lumen diameter] / vessel diameter). 20 vessels <200 μm per animal were analyzed. Representative images for each group are shown in upper panel. Size bars = 50 μm. Quantification is shown in lower panel. *p<0.05 vs control by one-way ANOVA with Tukey post-hoc correction. Each data point represents one animal. Error bars represent means ± SEM.

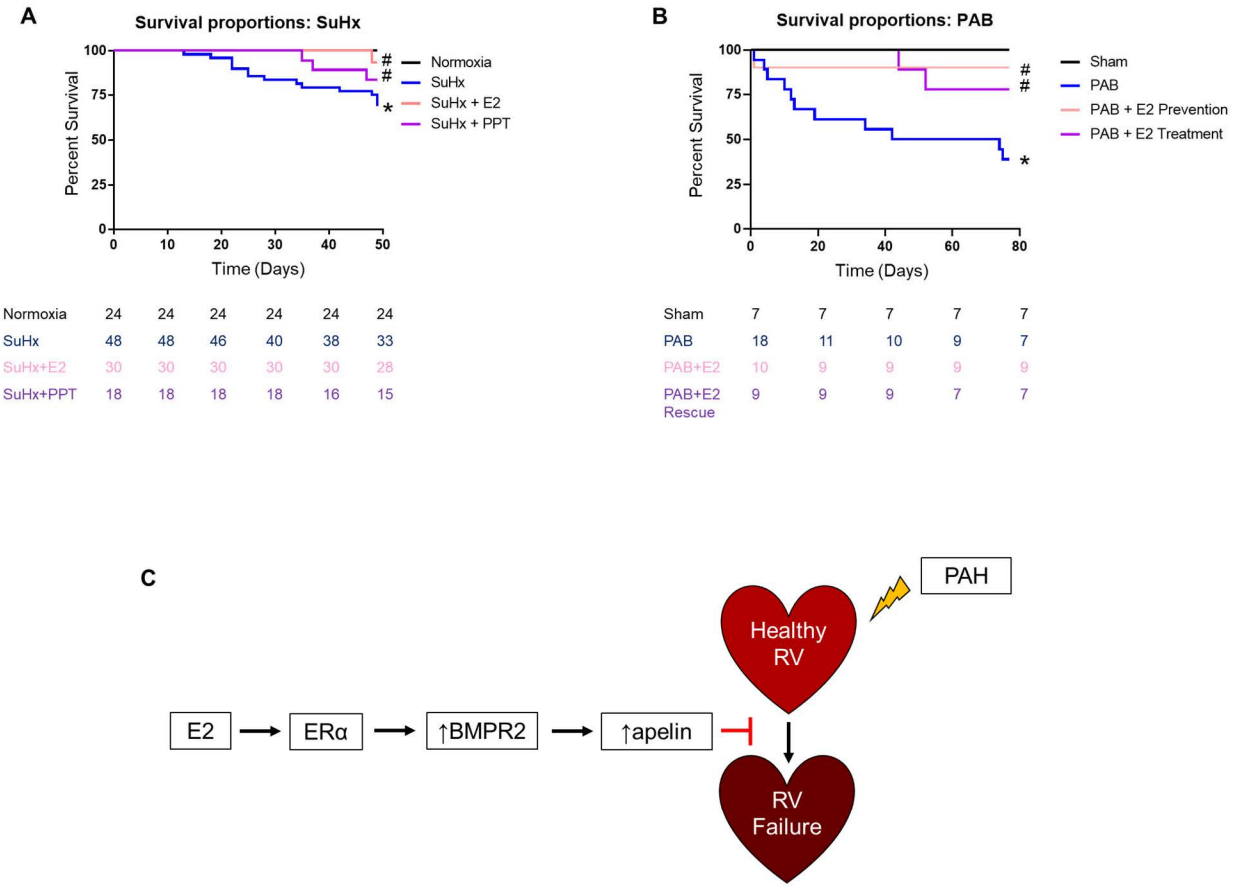

678

679 **Supplemental Figure 15: Effects of E2 or PPT treatment on survival in SuHx-PH or**
680 **pulmonary artery banding (PAB).** (**A**) Male Sprague-Dawley rats were treated with E2 (75
681 µg/kg/day via subcutaneous pellets) or PPT (850 µg/kg/day via subcutaneous pellets) starting
682 one week prior to SuHx induction. Premature mortality at seven weeks after SuHx initiation was
683 15/48 (31.2%) in the untreated SuHx-PH group, 2/30 (6.6%) in the SuHx+E2 group, and 3/18
684 (14.3%) in the SuHx+PPT group ($p<0.05$ by Log-rank [Mantel-Cox] test). (**B**) Male Sprague-
685 Dawley rats were treated with E2 (75 µg/kg/day via subcutaneous pellets) starting at the time of
686 PAB. Premature mortality at eleven weeks after PAB initiation was 11/18 (61.1%) in the untreated
687 PAB group, 1/10 (10%) in the PAB+E2 prevention group, and 2/9 (22.2%) in the PAB+E2 rescue
688 group. Numbers below graphs indicate animals at risk for corresponding time point. *$p<0.05$
689 vs normoxia control or sham, #$p<0.05$ vs. untreated SuHx or PAB by Log-rank [Mantel-Cox] test.
690 (**C**) depicts summary of experimental findings described in this manuscript.

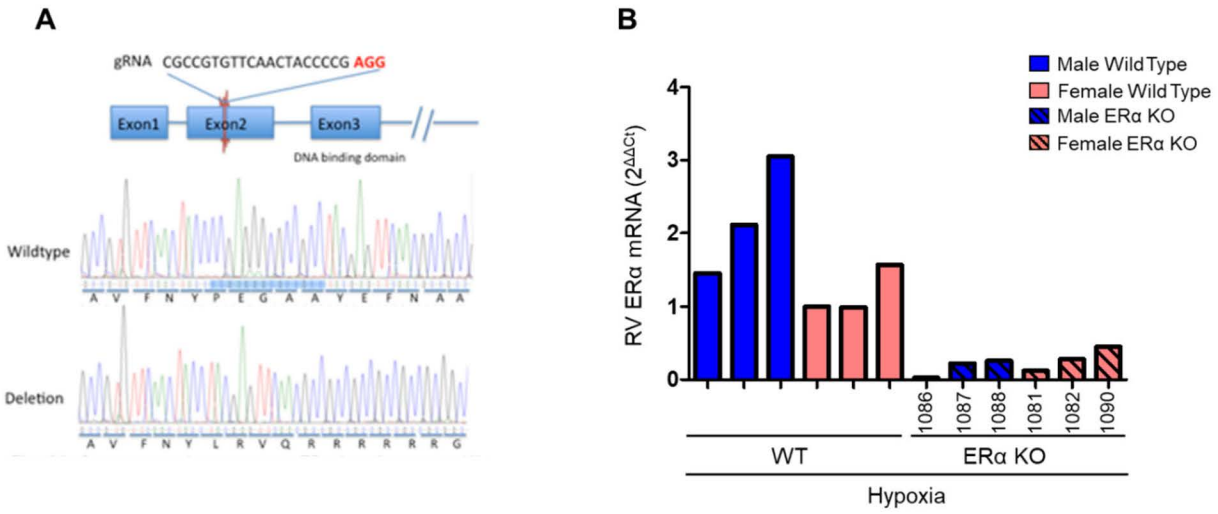

691

692

693

694 **Supplemental Figure 16: ERα mRNA expression is decreased in ERα (*Esr1*) mutated**
695 **Sprague-Dawley rats.** ERα mRNA expression by quantitative RT-PCR in ERα (*Esr1*) mutated
696 rat RVs. Animal numbers correspond with animal numbers in Supplemental Table 1. Relatively
697 higher apelin expression was noted in rats with mutations predicted to be heterozygous or
698 hypomorph, suggesting partial expression or function of ERα may be sufficient to increase apelin.

699

700

701

702

703

704

705

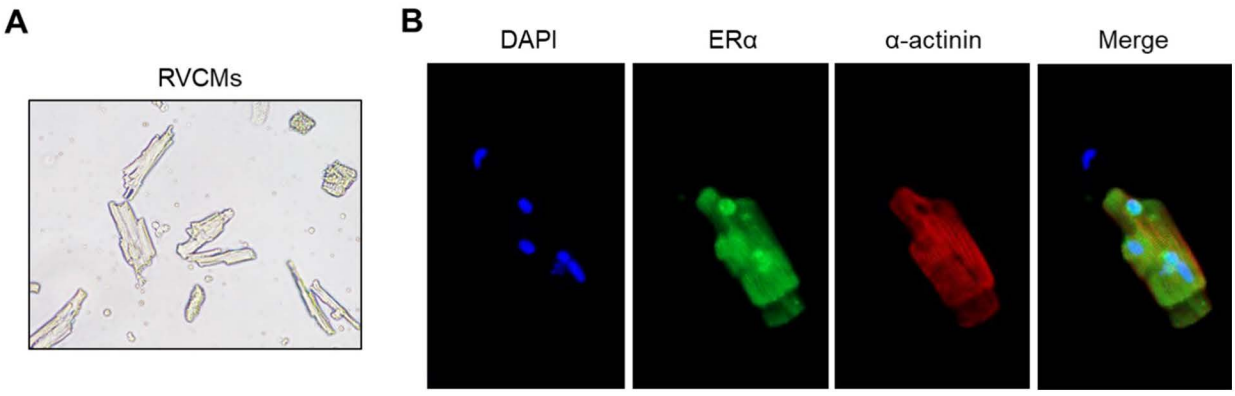

706

707

708 **Supplemental Figure 17: Rat RV cardiomyocyte (RVCM) isolation.** A viable cardiomyocyte
709 phenotype was confirmed by striated pattern, rectangular shape and α-actinin expression. (**A**)
710 Brightfield image of isolated RVCMs. Note striated pattern and rectangular shape of
711 cardiomyocytes. (**B**) ERα is expressed in rat RVCMs. Immunoflourescence staining for ERα
712 expression (green), α-actinin (red), and DAPI (nuclei; blue). Images taken at 40x.

713

714

715

716

717

718

719

720

721